Acta Crystallographica Section D
Biological Crystallography
ISSN 0907-4449

Structural adaptation of an interacting non-native C-terminal helical extension revealed in the crystal structure of NAD$^+$ synthetase from *Bacillus anthracis*

Heather M. McDonald,[a,b] Pamela S. Pruett,[a] Champion Deivanayagam,[a,c] Irina I. Protasevich,[a] W. Michael Carson,[a] Lawrence J. DeLucas,[a,b] Wayne J. Brouillette[a,d] and Christie G. Brouillette[a,d]*

[a]Center for Biophysical Sciences and Engineering, University of Alabama at Birmingham, Birmingham, Alabama 35294-4440, USA, [b]Department of Optometry, University of Alabama at Birmingham, Birmingham, Alabama 35294-4440, USA, [c]Department of Vision Sciences, University of Alabama at Birmingham, Birmingham, Alabama 35294-4440, USA, and [d]The Department of Chemistry, CBSE 234, University of Alabama at Birmingham, 1530 3rd Avenue South, Birmingham, Alabama 35294-4440, USA

Correspondence e-mail: christie@uab.edu

Received 5 March 2007
Accepted 18 June 2007

PDB References: NAD$^+$ synthetase, 2pzb, r2pzbsf; complex with AMP and pyrophosphate, 2pza, r2pzasf; complex with adenosine 5′-(α,β-methylene)triphosphate, 2pz8, r2pz8sf.

The crystal structures of NH_3-dependent NAD$^+$ synthetase from *Bacillus anthracis* as the apoenzyme (1.9 Å), in complex with the natural catalytic products AMP and pyrophosphate (2.4 Å) and in complex with the substrate analog adenosine 5′-(α,β-methylene)triphosphate (2.0 Å) have been determined. NAD$^+$ synthetase catalyzes the last step in the biosynthesis of the vitally important cofactor NAD$^+$. In comparison to other NAD$^+$ synthetase crystal structures, the C-terminal His-tagged end of the apoenzyme adopts a novel helical conformation, causing significant compensatory changes in the region. The structural accommodations observed in *B. anthracis* NAD$^+$ synthetase are remarkable in the absence of adverse affects on enzyme activity. They also illustrate a rare example of the influence of a non-native C-terminal His-tag extension on the structure of a native protein. In contrast to the apoenzyme, when AMP and pyrophosphate or adenosine 5′-(α,β-methylene)triphosphate are bound, the C-terminus adopts a conformation that allows ATP binding and overall the structure then resembles other NAD$^+$ synthetase structures. The structures of NAD$^+$ synthetase complexes from *B. anthracis* are compared with published X-ray crystal structures of the enzyme from *B. subtilis*, *Escherichia coli* and *Helicobacter pylori*. These comparisons support the novel observation that P1 and P2 loop ordering is not a consequence of crystal contacts but rather a consequence of intrinsic intramolecular interactions within the ordered subunit.

1. Introduction

NAD$^+$ synthetase (NADS) catalyzes the last step in the production of nicotinamide adenine dinucleotide (NAD$^+$) in both the *de novo* and pyridine nucleotide-salvage pathways in bacteria. NAD$^+$ is a ubiquitous coenzyme that is involved in various metabolic processes such as calcium mobilization, DNA repair, energy metabolism and signal transduction and is essential for both prokaryotic and eukaryotic organisms. The enzyme is also required for bacterial spore germination and outgrowth (Spencer & Preiss, 1967; Magni *et al.*, 1999; Rizzi & Schindelin, 2002).

Bacillus anthracis is a Gram-positive spore-forming bacteria and the causative agent of anthrax (McDevitt *et al.*, 2002; Shailubhai, 2003). NADS is a potential target for the development of antibiotics to treat anthrax, which is the primary reason for solving its structure (Velu *et al.*, 2003, 2005). NADS from *B. anthracis* catalyzes the amidation of nicotinic acid adenine dinucleotide (NaAD) in the presence of Mg^{2+} ions with substrates ATP and NH_3 to yield NAD$^+$, adenosine 5′-monophosphate (AMP) and pyrophosphate (PP_i), as shown in Fig. 1.

Structural information on NH_3-dependent NADS and its complexes with natural substrates, the NAD-adenylate intermediate and products has been obtained using X-ray crystallography (Devedjiev *et al.*, 2001; Jauch *et al.*, 2005; Kang *et al.*, 2005; Rizzi *et al.*, 1996, 1998; Symersky *et al.*, 2002). Structural investigations suggest a catalytic mechanism in which an adenylated NaAD reaction intermediate is formed from the ATP and NaAD substrates (Rizzi *et al.*, 1998). This process involves at least two Mg^{2+} ions which stabilize the active site of the enzyme by coordinating to active-site residues and to the ATP substrate. The functional unit of the enzyme is a compact homodimer with an α/β topology and an extensive monomer–monomer interface. The ATP-binding site is located at the classical α/β switch point, whereas the NaAD-binding site is found in an adjacent cleft that extends across the monomer–monomer interface. There are two NaAD-binding sites and two ATP-binding sites per dimer (Devedjiev *et al.*, 2001). To date, crystal structures of NADS from *B. subtilis* (*bsu*NADS), *Escherichia coli* (*eco*NADS) and *Helicobacter pylori* (*hpy*NADS) have been reported. Here, we present the structure of NADS from *B. anthracis* (*ban*NADS) in its apoenzyme form, in complex with the natural products AMP and PP_i and in complex with the substrate analog adenosine 5′-(α,β-methylene)triphosphate (AMP-CPP). The structural differences observed between the apoenzyme form and the *ban*NADS complex structures are discussed. In particular, the similarities between the *ban*NADS complex structures and those of *bsu*NADS, *eco*NADS and *hpy*NADS suggest that the novel structure of the *ban*NADS apoenzyme results from systematic accommodation to the interactions between the core of the protein and the helical C-terminal His tag.

2. Experimental procedures

2.1. Cloning, expression and purification

The *nadE* sequence gene of *B. anthracis* (accession No NP_844403, version NP_844403.1, gi:30262026, Entrez Gene GeneID 1087061; Read *et al.*, 2003) was used to design primers for two sequential rounds of PCR amplification. Initial PCR primers were used to amplify the *nadE* gene from the genomic DNA template (obtained from the Sterne strain) and also to add 5′ *Nde*I and 3′ *Hin*dIII sites: NADS_Forward, 5′-CATATGACATTACAAGAACAGATTATG-3′; NADS_Reverse, 5′-AAGCTTCCACCAATCATCAAACATTGA-3′. A second round of PCR primers were then used to re-amplify the first PCR product: NADS2_Forward, 5′-GGAGATATACATATGACATTACAAG-3′; NADS2_Reverse, 5′-GTGCGGCCGCAAGCTTCCACCAATC-3′. The PCR reaction mixture

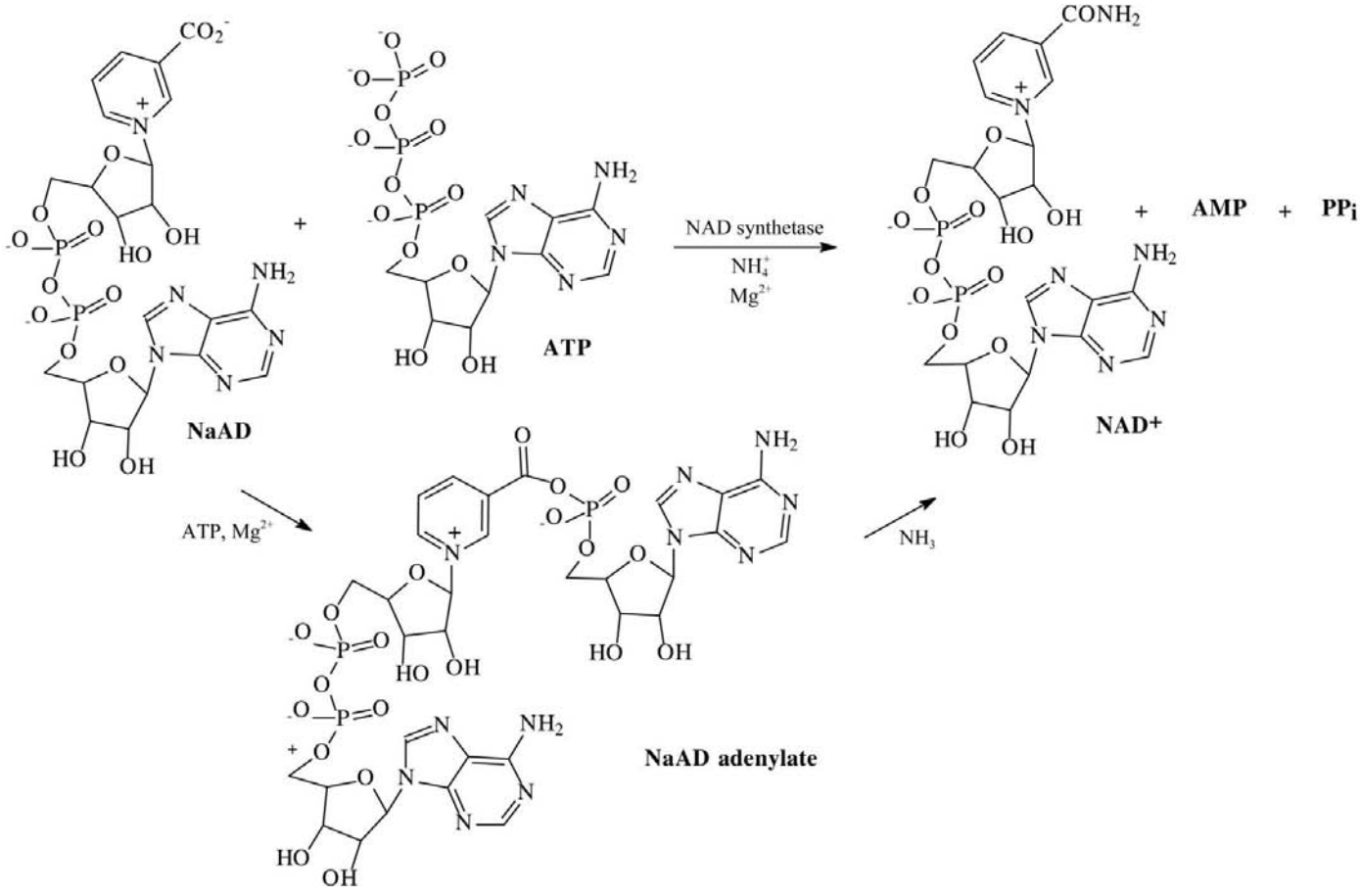

Figure 1
Amidation of nicotinic acid adenine dinucleotide (NaAD) catalysed by NAD synthetase (NADS) from *B. anthracis*.

contained Roche PCR mix containing nucleotides and Taq polymerase, 50 ng DNA and 1 μ*M* of each primer.

PCR products were purified using a PCR spin-prep kit (Novagen), digested with *Nde*I/*Hin*dIII (NEB), purified from an agarose gel using a spin column DNA-purification kit (Novagen) and ligated into pET21b using Clonables 2× Ligation mix from Novagen. Using this vector, a C-terminal fusion of 12 amino acids including a His_6 tag was incorporated into the expressed protein in order to facilitate purification. The ligated plasmid DNA was used to transform NovaBlue cells by heat shock at 315 K. Transformed cells were plated on Luria agar plates containing 50 μg ml^{-1} ampicillin. Mini-plasmid kits (Qiagen) were used to extract plasmid DNA from multiple colonies for sequence analysis by the CFAR sequencing core facility, UAB.

Plasmid with the correct sequence was used to transform BL21(DE3)pLysS (Novagen) for expression. Cells from a 2 l overnight growth were harvested by centrifugation and resuspended in 35 ml 20 m*M* sodium phosphate pH 7.2, 500 m*M* NaCl, 10 m*M* imidazole with protease-inhibitor cocktail. Following cell disruption, the supernatant was filtered and loaded onto a 5 ml Ni HiTrap column equilibrated with binding buffer (20 m*M* sodium phosphate pH 7.2, 500 m*M* NaCl, 10 m*M* imidazole). The column was eluted with 20 m*M* sodium phosphate pH 7.2, 500 m*M* NaCl, 500 m*M* imidazole using a linear gradient of 50–500 m*M* imidazole. Fractions containing the protein were pooled and concentrated and the buffer was exchanged to gel-filtration buffer (50 m*M* Tris pH 7.5, 0.1 *M* NaCl, 0.1 m*M* AEBSF, 1 m*M* DTT, 1% glycerol). The protein sample was then loaded onto an Amersham Biosciences Superdex-200 (or Superdex-75) column equilibrated with the same buffer. The NADS fractions were checked by SDS–PAGE and by activity assay and stored at 253 K in 50 m*M* Tris, 1 m*M* EDTA, 1 m*M* DTT, 0.1 m*M* AEBSF, 0.1 m*M* NaCl and 50% glycerol. All properties of the enzyme reported here are for enzyme that contains the C-terminal fusion of 12 amino acids (MW = 63 242 Da). Prior to each experiment, protein solutions were dialyzed into the desired buffer. The protein concentration was calculated based on $OD_{280\,nm}$ using an extinction coefficient of 0.728 cm^{-1} mg^{-1} ml.

2.2. pH-optimum experiments

The NADS reaction was coupled with the enzyme alcohol dehydrogenase (ADH), using the formation of product NADH to monitor the reaction at OD 340 nm (Bergmeyer, 1974). EPPS buffer (Sigma) at a final concentration of 60 m*M* and pH 6.5–9 in 0.5 pH units was used to determine the optimum pH for the activity of *bsu*NADS and *ban*NADS; other buffer components included 20 m*M* ammonium chloride, 20 m*M* potassium chloride, 10 m*M* magnesium chloride, 1% ethanol, 50 μg ml^{-1} ADH, 2 μg ml^{-1} NADS, 2 m*M* NaAD and 2 m*M* ATP. These experiments were conducted at 298 K for 30 min and then quenched with 6 *M* guanidine–HCl.

2.3. $K_{m(app)}$ determination

The substrate $K_{m(app)}$ values for ATP and NaAD were determined by an end-point assay (Zalkin, 1985), using for the most part the conditions used by Nessi *et al.* (1995) so that the present K_m values could be directly compared with those obtained previously for *bsu*NADS. As in the pH studies, the ADH-coupled assay was used to monitor product formation. The reaction buffer includes 60 m*M* EPPS pH 8.5, 20 m*M* ammonium chloride, 20 m*M* potassium chloride, 10 m*M* magnesium chloride, 1% ethanol, 50 μg ml^{-1} ADH, 6 μg ml^{-1} NADS (except for *bsu*NADS with ATP as the substrate, which used 2 μg ml^{-1} NADS) and 2 m*M* of one substrate held at a constant saturating concentration, while the other substrate was titrated over a range of concentrations from 0.03 to 2.5 m*M*. All components except ATP were mixed and placed in a 96-well microtiter plate. The plates were equilibrated at 310 K before the reaction was initiated by addition of ATP. After initiation, the reaction proceeded for 5 or 30 min and was then terminated by the addition of 6 *M* guanidine–HCl.

The $K_{m(app)}$ values were determined by Lineweaver–Burke double-reciprocal plots of 1/[*S*] *versus* 1/Abs(*V*), where the intercept on the *x* axis is $-1/K_{m(app)}$, or with nonlinear regression analysis using the Solver function in *Excel*.

2.4. Circular dichroism (CD)

CD spectra were recorded on an Olis DSM 1000 CD spectrophotometer (USA). The cells had a path length of 0.02 cm for protein concentrations of 0.23–0.33 mg ml^{-1}. Ten spectra were usually taken sequentially and were recorded from 260 to 203 nm in 1 nm steps. These ten spectra were then averaged to produce a single experimental spectrum; the molar ellipticity values were calculated according to the expression $[\Theta] = (\Theta/10)(\mathrm{MRW}/lc)$, where Θ is the ellipticity in millidegrees, MRW is the mean residue molecular weight in grams per mole (110.9), l is the path length in centimetres and c is the concentration of the protein in grams per litre. The value $[\Theta]$ has units of $^\circ$ cm^2 dmol^{-1}. In Fig. 5, the average of two different CD experimental spectra are shown that were obtained using different lots and at different times. The secondary-structure contents were obtained by deconvolution of CD spectra from 205 to 260 nm using software developed by Gerald Böhm (Böhm *et al.*, 1992).

2.5. Crystallization and data collection

The *ban*NADS apoenzyme was crystallized in hanging drops by vapor diffusion at 277 K against 8–12% PEG 8000, 0.505 *M* ammonium sulfate, 6% glycerol, 100 m*M* magnesium chloride, 0.05% *n*-octyl-β-D-glucopyranoside, 100 m*M* HEPES pH 7 with a drop volume ratio of 1:1 (18 mg ml^{-1} protein: reservoir). Crystals (form I) appeared in a week. Crystals of the complex of *ban*NADS with AMP and PP_i (form II) were obtained by cocrystallization with 0.5 m*M* NaAD and 1 m*M* ATP. Crystals of the complex of *ban*NADS with AMP-CPP (form III) were obtained by cocrystallization with 2 m*M* AMP-CPP; the crystallization conditions for the complexes were otherwise the same as those for the apoenzyme. Cryo-

Table 1
Crystallographic data.

Values in parentheses are for the highest resolution shell.

	Form I	Form II	Form III
Complex	—	AMP and PP_i	AMP-CPP
Space group	$P2_12_12_1$	$P2_12_12$	$P2_12_12$
Unit-cell parameters			
a (Å)	84.4	107.0	107.2
b (Å)	84.6	96.4	96.5
c (Å)	245.4	68.6	68.6
$\alpha = \beta = \gamma$ (°)	90	90	90
PDB code	2pzb	2pza	2pz8
Data collection			
Resolution (Å)	36.1–1.9 (1.97–1.90)	24.8–2.4 (2.49–2.40)	37.0–2.0 (2.07–2.00)
Unique reflections	131948 (13773)	28233 (2788)	48827 (4802)
Average redundancy	4.24 (3.22)	2.9 (2.9)	7.0 (6.2)
Completeness (%)	95.0 (90.5)	99.1 (99.3)	99.9 (99.6)
R_{sym} (%)	6.3 (28.1)	5.5 (18.7)	8.8 (40.2)
$I/\sigma(I)$	14.8 (3.3)	19.6 (3.5)	14.9 (3.2)
Refinement			
Protein molecules in ASU	4	2	2
R_{work}/R_{free} (%)	21.9/23.7	21.6/25.9	20.2/22.9
Average temperature factors (Å^2)			
Protein	36.0	18.3	23.5
Water O atoms	39.4	25.9	29.1
Ligands	41.5†	16.7	21.0
Wilson B factor	36.2	19.1	24.5
Ramachandran analysis			
Allowed (%)	100	100	100
Favored (%)	98.8	98.6	99.5
Outliers	0	0	0
R.m.s. deviation from ideal values			
Bond length (Å)	0.006	0.008	0.007
Bond angle (°)	1.1	1.3	1.2

† Ligands for form I refer to the three bound sulfate anions per monomer.

protection solutions were obtained by adding glycerol to hanging drops that failed to yield crystals such that the final glycerol concentrations were 5, 10, 15, 20 and 25%. These solutions were then used to sequentially soak crystals of *ban*NADS in increasing amounts of glycerol for 30 s per drop. The crystals were then flash-frozen in a cryostream at 93 K for data collection. Attempts to cryoprotect crystals in solutions that did not contain *ban*NADS resulted in cracking or dissolution of crystals.

Diffraction data from the apoenzyme crystal were collected at SER-CAT at the Advanced Photon Source using synchrotron radiation at a wavelength of 1 Å and a MAR 300 detector. Diffraction data from crystal forms II and III were collected using a Rigaku (Tokyo, Japan) rotating-anode X-ray generator equipped with an R-AXIS IVB image plate. Data were processed with the *DENZO* and *SCALEPACK* software package (Otwinowski & Minor, 1997).

2.6. Structure solution, refinement and modeling

The apoenzyme structure was solved by molecular replacement (MR) using the software program *Phaser* (McCoy *et al.*, 2005) and the *CCP*4*i* program interface (Potterton *et al.*, 2003). The MR search model of *ban*NADS was generated using the program *SWISS-MODEL* (Schwede *et al.*, 2003) and was derived from the published *bsu*NADS structure (PDB code 1ee1) coordinates. The MR solution was subject to rigid-body refinement, conjugate-gradient minimization and simulated annealing using *CNS* (Brünger *et al.*, 1998), with 10% of reflections set aside to monitor R_{free}. *ARP*/*wARP* (Morris *et al.*, 2003) was used to improve the phases and electron density of the model and further model building was carried out using *O* (Jones *et al.*, 1991). $F_o - F_c$ electron-density maps indicated the presence of positive difference density and sulfate ions were added to the model, which was then further refined. During the last cycles of refinement, water molecules were added. The other *ban*NADS structures were solved by molecular replacement with *Phaser* (McCoy *et al.*, 2005; Potterton *et al.*, 2003) using *ban*NADS apoenzyme as the search model and were refined as outlined above. During refinement, clear difference density appeared for the P1 and P2 loops, residues 257–265, ligands and ions, which were modeled. The final geometries of the models were evaluated using *MolProbity* (Lovell *et al.*, 2003).

Secondary-structure analysis was performed using *PROMOTIF* (Hutchinson & Thornton, 1996) and buried surface area was estimated using the Protein–Protein Interaction Server (Jones & Thornton, 1996). Figures of protein structures were created using the molecular-graphics programs *PyMOL* (DeLano, 2002) and *Ribbons* (Carson, 1997).

3. Results

3.1. Expression, purification and enzymatic characterization of expressed *ban*NADS

The nadE open reading frame from *B. anthracis* was amplified by PCR, with restriction sites included for cloning into the pET21b vector as described in §2. The protein was overexpressed in *E. coli* and purified by Ni^{2+} metal-chelation and size-exclusion chromatography.

The pH optimum for catalytic activity of *ban*NADS was determined and compared with that of *bsu*NADS. Both have an optimum pH near 8, as shown in Fig. 2. A range of 8.2–8.7 was previously reported for the *bsu*NADS pH optimum (Nessi *et al.*, 1995). The $K_{m(app)}$ values for NaAD and ATP were determined to be 152 and 289 μ*M*, respectively, for *ban*NADS. These are similar to those obtained for *bsu*NADS, 179 and 196 μ*M*, respectively, which in turn are nearly the same as the previously reported values of 280 and 210 μ*M* for *bsu*NADS using essentially the same protocol (Nessi *et al.*, 1995; see §2

for details). The slightly higher ATP $K_{m(app)}$ for *ban*NADS may be related to the conformational change deemed necessary for binding substrates, which is inferred from the apoenzyme structure (see below for details).

3.1.1. Apoenzyme crystal structure. The crystal structure of the *ban*NADS apoenzyme (form I; Table 1) was determined by molecular replacement using a *ban*NADS search model obtained using *SWISS-MODEL* (generated from the *bsu*NADS structure, PDB code 1ee1; see §2). Two dimers are observed in the asymmetric unit, corresponding to a calculated Matthews coefficient of 3.5 Å^3 Da^{-1} and a solvent content of 65.3%. The final structure was refined to 1.9 Å resolution with an R factor of 21.9% and an R_{free} of 23.7%. The crystallization construct consisted of the native protein, residues 2–272, and a C-terminal hexahistidine tag with linker, residues 273–284. All residues had well defined electron density except for 85–87 (P1 loop), 206–226 (P2 loop), 257–265 and the last histidine of the His tag, His284. It may be worth noting that not all molecules in the asymmetric unit showed electron density for Met1, Val84, Glu88 and His83. In addition, electron density was present for Ala264 and Ser265 in one of the molecules in the asymmetric unit. The *ban*NADS structure has α/β folds similar to the *B. subtilis* enzyme; the core of the *ban*NADS enzyme exhibits a typical Rossmann fold. A sequence alignment based on structural homologies is shown in Fig. 3 (the PDB codes of the structures used are given in the legend) and ribbon representations of the apoenzyme are shown in Figs. 4(*a*) and 4(*b*). The apoenzyme structure of *ban*NADS is 51% α-helical and 6% β-sheet in conformation. It is interesting that these values are also in close agreement with circular-dichroism measurements (Fig. 5), *i.e.* deconvolution of the far-UV spectrum of *ban*NADS indicates that it is 51.5% helical in solution. A helical content of 47% was calculated for the apoenzyme structure with a nonhelical C-terminus. While the helicity in solution measured by CD is closer to that of the apoenzyme with a helical C-terminus, care must be exercised in putting too much weight on the CD value since CD spectra lack definition and deconvolution algorithms can only provide an approximate value for the absolute amount of secondary structure. Therefore, it is possible that the C-terminal helix is not present in solution and is only a consequence of crystallization. Each monomer has approximately 1873 Å^2 of buried surface area at the dimer interface, which constitutes 14.4% of the total accessible surface area of the molecule as seen in the crystal structure. These dimer-interface interactions are primarily mediated by the α5 and the α6 helices. Analysis using *MolProbity* (Lovell *et al.*, 2003) shows good stereochemistry: 100% of all residues are in allowed regions of the Ramachandran plot, with 98.8% of residues in favored regions. The *ban*NADS apoenzyme crystal structure contains three sulfate ions per monomer. One of the sulfate ions is observed in the ATP-binding site (see below), a second interacts with

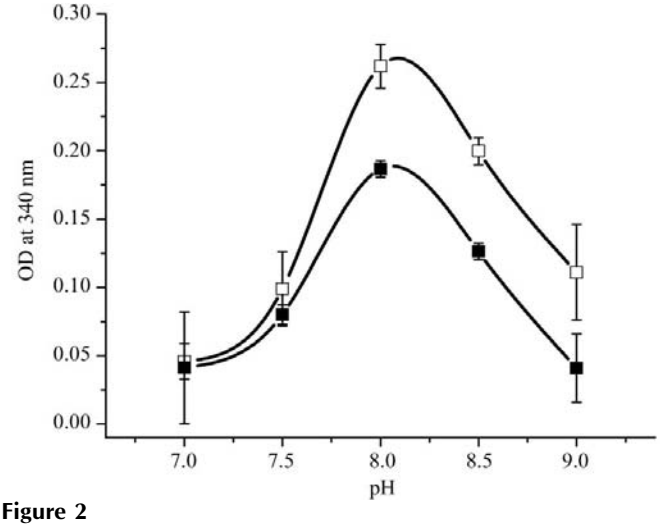

Figure 2
The pH optimum for *bsu*NADS *and ban*NADS. Each data point represents the average of three replicates; error bars on all points are standard deviations. The plot for *bsu*NADS is depicted with open squares and that for *ban*NADS is depicted with closed squares.

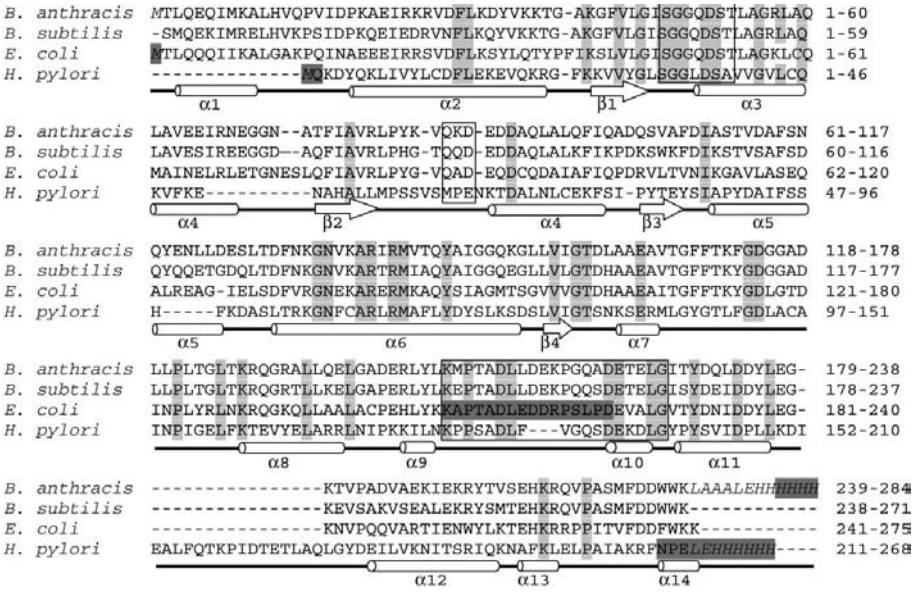

Figure 3
Structural alignment of NADS taken from substrate complexes of *B. anthracis*, *B. subtilis*, *E. coli* and *H. pylori* using the structure of *ban*NADS form II and the structures 1ee1, 1wxh and 1xng from the PDB, respectively. The alignment was generated using *MODELLER* (Sali & Blundell, 1993). Light gray highlighting designates conserved residues and dark gray highlighting designates residues that are absent from the crystal structure. Secondary-structural elements correspond to the *ban*NADS complex structures. Residues enclosed in boxes are, as they appear in the sequence, the ATP pyrophosphatase fingerprint sequence, the P1 loop and the P2 loop, respectively. Italics designate non-native residues. Note: The *ban*NADS complex structure α13 is a 3_{10}-helix. See supplementary Table 2 for the specific substrates involved in each complex.

Lys136 and Arg140 in helix α6 and the third interacts with the main-chain N atom of Phe130 (near the N-terminal end of the α6 helix; the helices are labeled in Figs. 3 and 4) and the His-tag residues His280 and His283.

3.1.2. Complex crystal structures. The structures of the enzyme complexes with the natural catalytic products AMP and PP_i (form II) and the substrate analog AMP-CPP (form III) were determined in a similar manner as outlined for the apoenzyme. Figs. 4(*c*) and 4(*d*) show the structure of the form III complex. The crystals of the enzyme complexes adopt space group $P2_12_12$ rather than that of the apoenzyme ($P2_12_12_1$). Both forms II and III contain one dimer in the asymmetric unit, corresponding to a Matthews coefficient of 2.8 $Å^3$ Da^{-1} and a solvent content of 55.6%. The structure of the form II complex was refined to 2.4 Å, with a final *R* factor of 21.6% and an R_{free} of 25.9%, and that of form III was refined to 2.0 Å resolution, an *R* factor of 20.2% and an R_{free} of 22.9% (Table 1). For both the form II and III complexes, clear electron density was observed for all residues except for the last four residues of the C-terminal His tag (His281–His284). The P1 loop (residues 85–87), the P2 loop (residues 206–226) and residues 257–265 are well ordered in both forms II and III. The root-mean-square (r.m.s.) deviation of an alignment of C^α atoms between the form II and III complexes is 0.42 Å, indicating close similarity in secondary and tertiary structure. The *ban*NADS complex is 52% α-helical and 6%

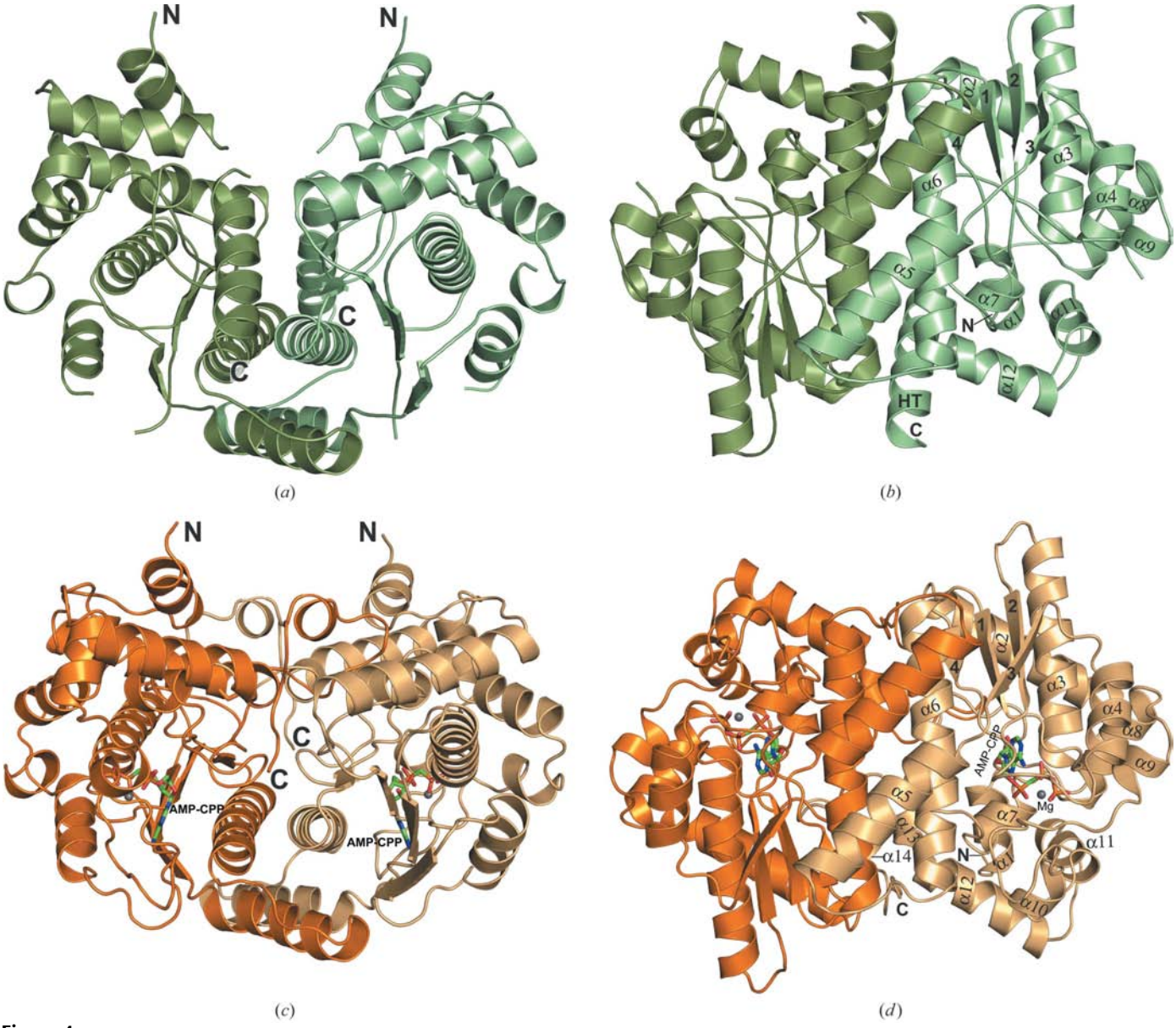

Figure 4
Structure of the *ban*NADS homodimer. (*a*), (*b*) Apoenzyme crystal. Monomers *A* and *B* are shown in green and light green, respectively. The N- and C-termini, α-helices (HT = His tag) and β-sheets are labeled. Note that electron density for α10 is missing in the apo structure. Sulfate ions are not shown. (*c*), (*d*) Complex with AMP-CPP (crystal form III). Monomers *A* and *B* are shown in orange and beige, respectively. The AMP-CPP molecules are shown in ball-and-stick representation and the Mg^{2+} ions are shown as gray spheres. N- and C-termini, α-helices and β-sheets are labeled. Glycerol molecules are not shown. (*b*) and (*d*) are rotated −90° about the *x* axis of the page with respect to (*a*) and (*c*).

β-sheet. There is approximately 3000 Å^2 buried surface area at the dimer interface per monomer, constituting 21.4% of the total accessible surface area, and as with the apoenzyme these interactions are primarily mediated by the α5 and α6 helices. The structural differences observed at the C-terminus of the apo and complex structures (described below) and the presence of ordered loop regions in the complex structure contribute to a higher buried surface area than in the apoenzyme. Both complex structures show good stereochemistry. For the form II complex 100% of the residues are in allowed regions of the Ramachandran plot, with 98.6% in favored regions. For the form III complex 100% of the residues are in allowed regions of the Ramachandran plot, with 99.5% in favored regions. Both ATP-binding sites of the functional dimer are occupied by the respective ligands: one AMP molecule, one PP_i ion and two Mg^{2+} ions in each monomer of the form II complex and one AMP-CPP molecule and one Mg^{2+} ion in each monomer of the form III complex. In addition, there is one glycerol molecule observed in each monomer of the structures of the form II and III complexes.

3.2. Description of the ATP-binding site

The addition of ATP and NaAD resulted in crystal form II, which contains AMP and PP_i, indicating that hydrolysis of ATP took place during crystallization; however, NaAD is not observed in the binding site. Clear electron density was observed for ligands bound in both the form II and III complexes as shown in Figs. 6(*b*) and 6(*c*) and supplementary Figs. 11(*a*) and 11(*b*)[1]. In both the form II and III complexes, the ribose portions of the ligand interact with the protein through hydrogen bonds to the backbone O atom of Gly45 (to ribose O2*) and the side-chain hydroxyl group of Thr158 (to ribose O3*), while stacking interactions are found between Ser47 and the adenine ring. Stabilization of the P1 loop is mediated by a hydrogen bond between N6 of the adenine moiety and Gln85 (Fig. 6*a*). Also, atom N1 of the adenine moiety participates in a hydrogen bond to a side-chain N atom of Arg79 and to the main-chain N atom of Leu80. An α-phosphate O atom hydrogen bonds to the backbone carbonyl O of Thr209, leading to stabilization of the P2 loop (Fig. 6*a*). Residues Ser47, Ser52, Gln50 and Lys187 hydrogen bond to the PP_i and AMP-CPP phosphate moieties.

In the existing published bacterial NADS crystal structures, three magnesium-binding sites (Mg^{2+}-I, Mg^{2+}-II and Mg^{2+}-III) have been identified. Supplementary Table 2[1] summarizes the pertinent details of the ATP-binding site in all NADS structures determined to date, including the presence of magnesium ions. The location of all three magnesium-binding sites is illustrated pictorially in Fig. 6(*a*). Occupancy of one or more of these sites occurs when an AMP or ATP ligand is bound in the ATP-binding site. However, all three sites have never been shown to be occupied in a single structure and furthermore there is no obvious structural explanation for why one may be occupied over another. Detailed comparisons will be made in §4. In both the form II and III complexes, Mg^{2+}-II is occupied and shows a typical octahedral coordination sphere (Fig. 6*b*). In the form II complex, this interaction is coordinated by an oxygen (O1P) from the AMP α-phosphate, the two phosphate groups of pyrophosphate, the backbone O atom of Thr209 and two water molecules. The other magnesium-binding site (Mg^{2+}-I) is only occupied in the form II complex and shows octahedral coordination by an oxygen (O3P) from the AMP α-phosphate, the two phosphate groups of pyrophosphate, the side-chain O atom of Glu163, the side-chain O atom of Asp51 and one water molecule (Fig. 6*c*).

It is interesting to note that in the apoenzyme structure a sulfate ion binds in the ATP-binding site and interacts with residues Ser47, Ser52, Thr158, Lys171 and a water molecule (Fig. 6*d*). The sulfate ion in the ATP-binding site of the apoenzyme (form I) is one of three sulfate ions found per monomer. Since phosphate and sulfate ions are sufficiently similar to allow the two groups to bind in locations with similar properties, it is not uncommon when crystallizing with high concentrations of ammonium sulfate for sulfate ions to bind in phosphate-binding sites (Copley & Barton, 1994).

3.3. Comparison of the *ban*NADS apoenzyme and complex structures

Aside from the disorder–order change in the P1 and P2 loops, which has been reported previously for *bsu*NADS and *eco*NADS (Rizzi *et al.*, 1996; Jauch *et al.*, 2005), the *ban*NADS apoenzyme structure shows several unexpected features in comparison to its complex structures and also in comparison to other NADS apoenzyme structures. The r.m.s. deviations of a C^{α} alignment of atoms of form I with form II and with form III are 1.18 and 1.16 Å, respectively (supplementary Table 3[1]).

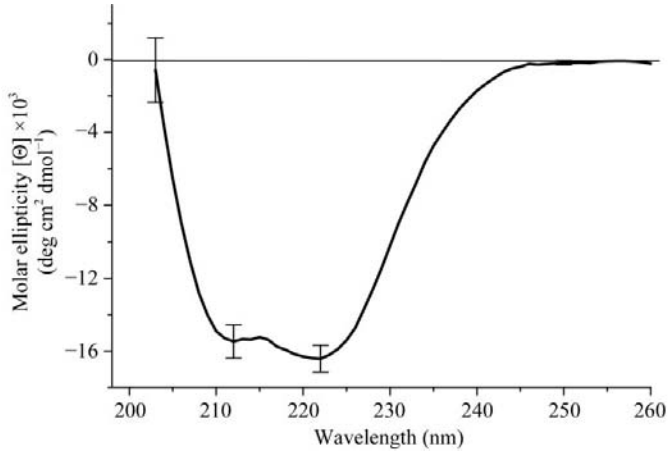

Figure 5
Circular-dichroism spectrum of *ban*NADS in the far-UV region. Spectra were obtained at 295 K in 60 m*M* EPPS pH 8.5, 20 m*M* potassium chloride, 19 m*M* ammonium chloride, 10 m*M* magnesium chloride. Depicted is the average of two spectra obtained from two different lots of *ban*NADS on different dates. To illustrate the variation in the measurement, error bars are shown at four different wavelengths representing the range of ellipticity values obtained for each spectrum used for the average.

[1] Supplementary material has been deposited in the IUCr electronic archive (Reference: EN5232). Services for accessing this material are described at the back of the journal.

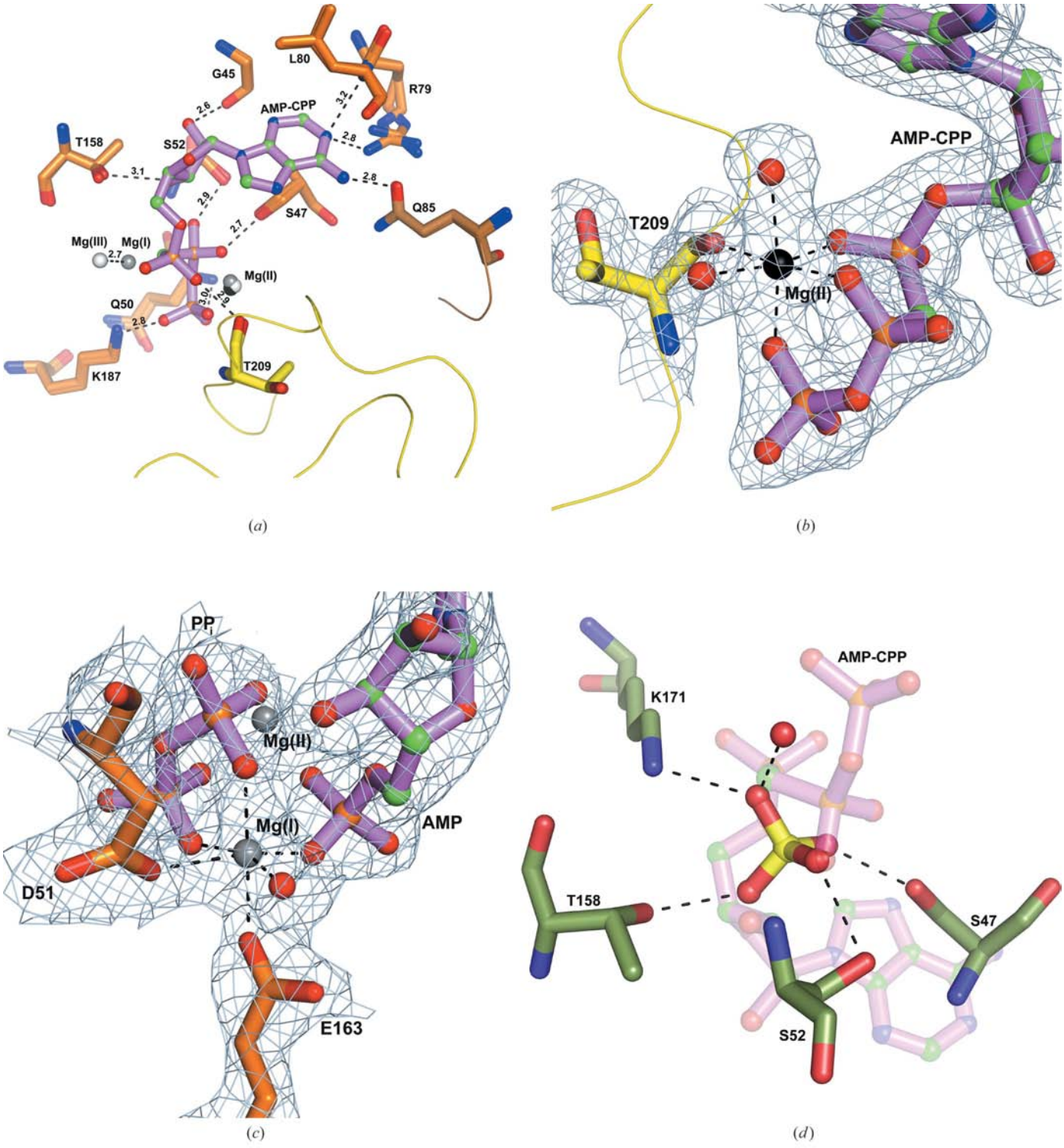

Figure 6
ATP-binding site overview. (*a*) Superposition of *ban*NADS (form III) and *bsu*NADS (PDB code 1ih8) active-site residues. ATP-binding site residues, shown as orange sticks (except for the P1 and P2 loops which are shown in brown and yellow, respectively) and labeled with *ban*NADS numbering. The *ban*NADS backbone of the P1 and P2 loops is shown as a ribbon and the AMP-CPP is shown in purple stick representation. The *ban*NADS Mg^{2+}-II ion is shown as a black sphere and the *bsu*NADS Mg^{2+}-II and Mg^{2+}-III ions are shown as white spheres. The Mg^{2+}-I and Mg^{2+}-II of the *ban*NADS form II complex are shown as gray spheres. Ball color by atom: nitrogen, blue; oxygen, red; carbon, green; phosphorus, orange; sulfate, yellow. Mg^{2+}-I, Mg^{2+}-II and Mg^{2+}-III are labelled Mg(I), Mg(II) and Mg(III), respectively, in this figure. (*b*) Mg^{2+}-II coordination in *ban*NADS form III; water molecules are shown as red spheres and $2F_o - F_c$ electron density at 1σ is shown in gray. Bond distances range from 2.0 to 2.2 Å. (*c*) Mg^{2+}-I coordination in *ban*NADS form II; AMP and PP_i are shown in purple stick representation and $2F_o - F_c$electron density at 1σ is shown in gray. Bond distances range from 2.1 to 2.4 Å. (*d*) ATP-binding pocket of *ban*NADS apoenzyme form I. Residues coordinated to sulfate ion are shown as green sticks. Bond distances range from 2.5 to 2.8 Å. Color by atom: nitrogen, blue; oxygen, red; sulfate, yellow. AMP-CPP ligand overlay from *ban*NADS form III is included as a transparent ball-and-stick representation.

For *bsu*NADS, *eco*NADS and *hpy*NADS, the r.m.s. deviations between their apoenzyme and complex forms are 0.50, 0.48 and 0.58 Å, respectively. While the r.m.s.d. of ∼1.2 Å is not much larger than ∼0.5 Å, it may point to some significant difference in either the *ban*NADS apoenzyme or complex in comparison to the homologous structures. In fact, the r.m.s.d. of ∼1.2 Å seems to result from the displacement of several secondary-structural elements in the *ban*NADS apoenzyme from their expected locations as found in *bsu*NADS apoenzyme, since complexes of *ban*NADS are much more similar to both the apo form and complexes of *bsu*NADS than the *ban*NADS apoenzyme is to either. Therefore, the apo *ban*NADS structure is unique in comparison to all other homologous NADS structures, including complexes of *ban*NADS itself. The unique regions will be described in the following sections and are shown sequentially in Fig. 7.

There are seven specific sequence spans in the *ban*NADS apoenzyme structure in which C^{α} atoms deviate by more than 1 Å in comparison to complexes of *ban*NADS. These seven discrete sequences comprise residues 1–16, 65–71, 88–92, 101–103, 158–176, 227–256 and 266–280. As designated by the two elliptical outlines in Fig. 7(*a*), these seven stretches of sequence are clustered in two different regions. One region is near the extreme C-terminus (at the top of the structure as oriented in Fig. 7*a*). Differences seen in this region are unique to *ban*NADS and result from the unusual conformation of the C-terminus in the apoenzyme, as described below (§3.4). The other region in which differences are observed is closer to the N-terminus and is apparently influenced by the presence or absence of the P1 loop, residues 85–87 (§3.5). Similar differences between the apoenzyme and complex structures are observed in *bsu*NADS and are discussed here for the first time.

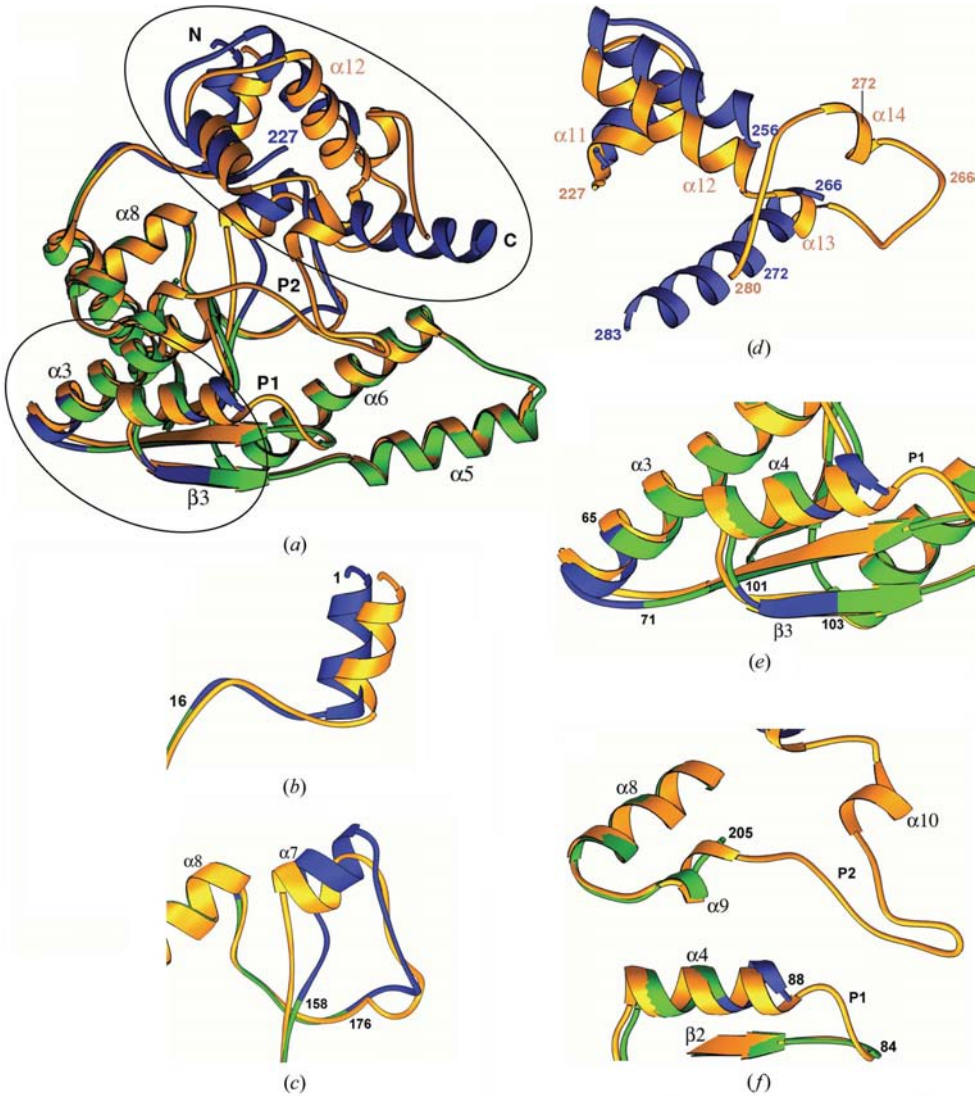

Figure 7
Comparison of *ban*NADS apo (form I) and complex (form III, orange) crystal structures. Form I is in green, except where the C^{α} r.m.s. deviation is >1 Å between forms I and III; these regions are shown in blue. Ligands are omitted for clarity. (*a*) Superposition of monomers. The orientation is rotated 50° about the *x* axis and 35° about the *y* axis of the page with respect to Figs. 4(*b*) and 4(*d*). (*b*) N-terminus. (*c*) Region 158–176. (*d*) C-terminal regions, residues 227–256 and 266–280; the orientation is rotated −90° about the *y* axis of the page compared with Fig. 6(*a*). (*e*) Regions 65–71 and 101–103. (*f*) The P1 and P2 loops. For comparison, only the form III complex structure is shown on the basis of its higher resolution (2.0 Å); otherwise, the protein structures of the form II and III complexes are practically identical.

3.4. Packing region near the extreme C-terminus

3.4.1. Helix *α*1, residues 1–16. The first 16 residues of the N-terminus of the apoenzyme are shifted away from the core structure compared with the form II and III complexes (Fig. 7*b*). The C^{α} position of the first residue is displaced by 5.3 Å and the distances between C^{α} atoms between the structures gradually decrease until residue 17, where the deviation is <1 Å. Region 1–16 tilts inward upon complex formation in an apparent rigid-body movement, maintaining its interactions with helices α11 and α12 (residues 227–256).

3.4.2. 'Inner loop', residues 158–176. This sequence forms a large irregularly shaped loop that includes the five-residue α-helix α7 (161–164). Residues within the loop that participate in binding both ATP and NaAD are Thr158 (ATP binding) and the NaAD-binding site residues Phe168, Phe169 and Lys171. Structural elements of the loop move by as

much as 3 Å upon complex formation (Fig. 7*c*). The movement and coincident small adjustments in conformation seems cooperative with the ordering of the P2 loop, which packs on top of it. In fact, the conformation of loop 158–176 in the apoenzyme does not allow room for the conformation adopted by the P2 loop in the complex form.

3.4.3. Helices α11 and α12, residues 227–256. Residues 227–256 are composed of two α-helices: α11 (229–236) and α12 (243–255). The latter helix shifts by ∼4 Å upon complexation (Fig. 7*d*). None of the residues in this region are involved in binding NaAD or ATP; however, they are contiguous and directly between two regions with dramatically different conformations in the apo and complex forms, *i.e.* the P2 loop (before residue 227) and the C-terminus starting with residue 257. Consequently, it is easy to imagine that the 'pull and tug' by these two flanking regions will be transmitted in

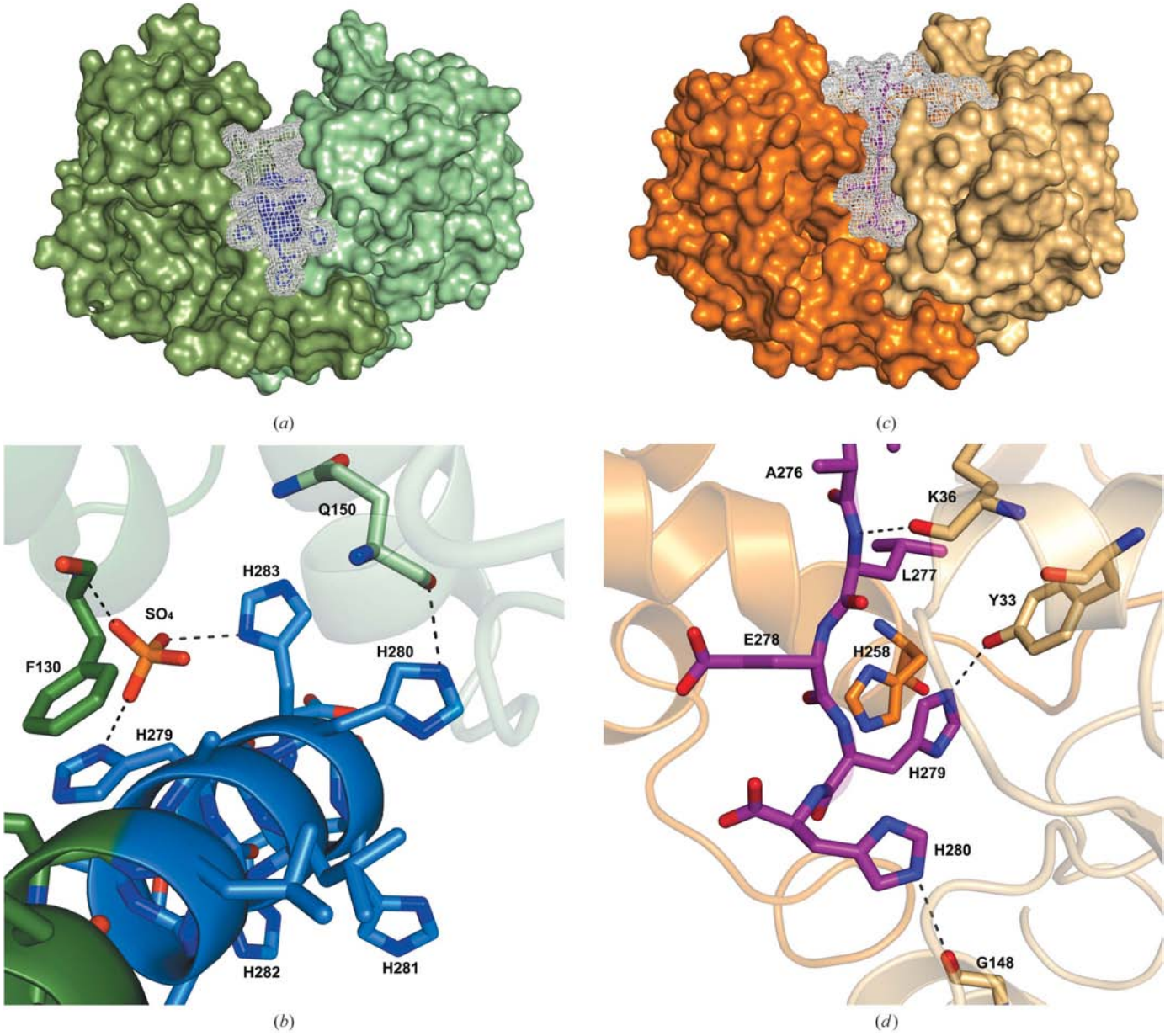

Figure 8
Surface representations of *ban*NADS in apo and complex forms, illustrating the interaction of the C-terminal His tag with the remainder of the protein. (*a*) Surface representation of *ban*NADS apoenzyme crystal structure. Monomers *A* and *B* are shown in green and light green, respectively. The C-terminal helix is shown in ribbon representation with stick side chains and mesh surface overlay. Non-native residues of monomer *A* are shown in blue. (*b*) Apoenzyme form I His-tag contacts with stick side chains. Color by atom: nitrogen, blue; oxygen, red; sulfur, orange. Contact distances range from 2.9 to 3.0 Å. (*c*) Surface representation of *ban*NADS form III complex. Monomers *A* and *B* are shown in orange and beige, respectively. The C-terminus is shown in ribbon representation with stick side chains and mesh surface overlay. Non-native residues of monomer *A* are shown in purple. Figs. 8(*a*) and 8(*c*) are shown in the same orientation as Figs. 4(*a*) and 4(*c*), respectively. (*d*) His-tag contacts in the form III complex. Contact distances range from 3.0 to 3.1 Å.

some way to cause a change in conformation or position of the intervening residues. In regard to packing interactions, helices

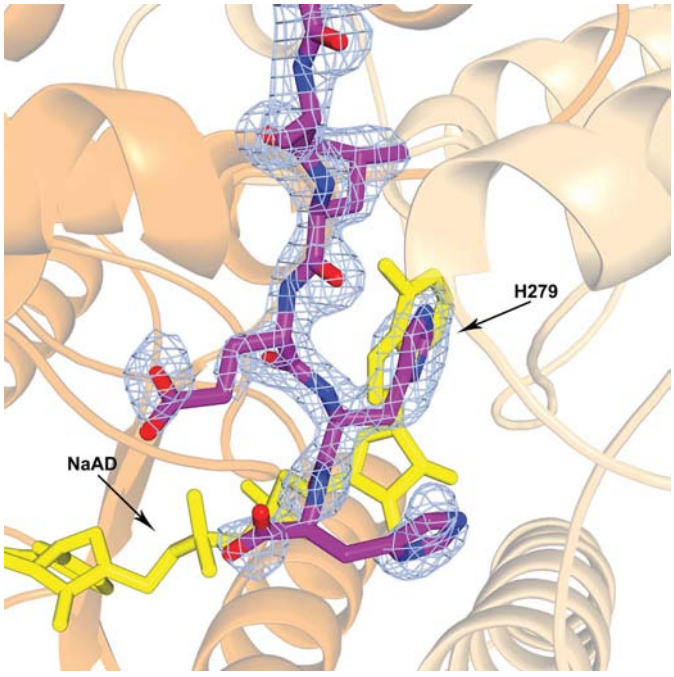

Figure 9
Partial NaAD-binding site of *ban*NADS crystal form III. Monomers *A* and *B* are shown in light orange and beige, respectively, and non-native C-terminal residues are shown in in purple. $2F_o - F_c$ electron density at 1σ is shown in gray. A superposition of the *bsu*NADS NaAD molecule from the NADS structure 1ee1 is shown as yellow sticks. The orientation is rotated 40° about the *x* axis and −15° about the *y* axis of the page with respect to Fig. 4(*c*).

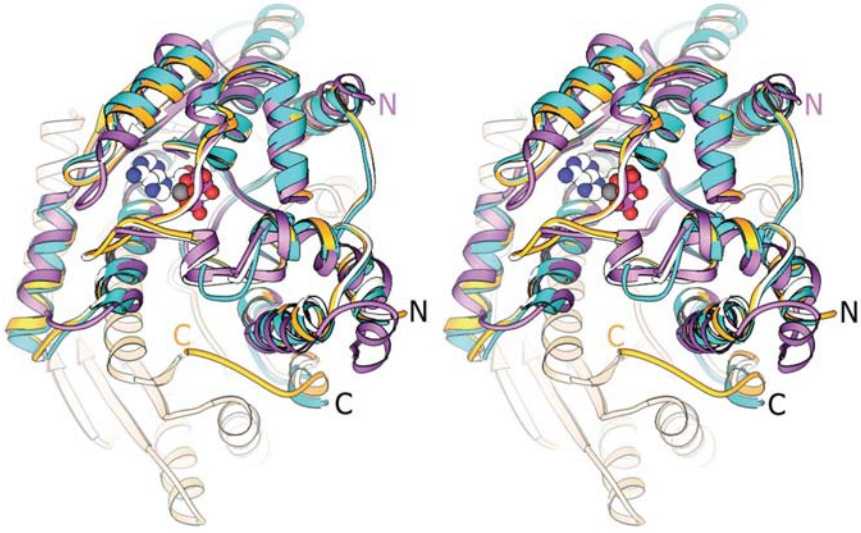

Figure 10
Phylogenetic comparison. Superposition of the *ban*NADS–AMP-CPP complex structure (molecule *A* is shown in orange and molecule *B* is shown in beige; form III) with the *bsu*NADS–AMP-CPP complex structure monomer (white; PDB code 1ih8), the *eco*NADS–AMP complex structure (blue; PDB code 1wxe) and the *hpy*NADS–ATP–NaAD complex structure monomer (pink; PDB code 1xng). The AMP-CPP and Mg^{2+} in *ban*NADS are shown as spheres (color by atom: nitrogen, blue; oxygen, red; carbon, white; phosphorus, pink; magnesium, black). The orientation is rotated 130° about the *z* axis and 90° about the *y* axis of the page with respect to Fig. 4(*d*).

α11 and α12 pack against each other and against helix α1 and helix α7, respectively.

3.4.4. C-terminal helix including His tag, residues 257–283. The apoenzyme C-terminal helix consists of native NADS residues to residue 272 followed by the non-native tag including five of the six histidines at residue positions 279–284. Electron density for native residues 257–265 and His284 is absent in the apoenzyme, whereas residues 281–284 are disordered in the form II and III complexes. The electron density missing for residues 257–265 in the apoenzyme *ban*NADS structure has been observed (*i.e.* is not missing) in the other known apoenzyme NADS crystal structures as well as the *ban*NADS complexes, suggesting that the structure of the His tag somehow prevents residues 257–265 from acquiring a stable conformation (Fig. 7*d*). A further difference between the two structural forms is the substantial switch in both the secondary structure and the position of residues 267–282 from a helix in the apoenzyme (form I) to largely random coil upon complex formation (forms II and III). The resulting movement of the C-terminus amounts to an 18 Å change in the location of Lys272. This change is illustrated in the ribbon representation of the region shown in Fig. 7(*d*). It is also represented in the surface representation of the apo and complexed enzymes shown in Figs. 8(*a*) and 8(*c*), respectively.

As can be seen in Fig. 8(*a*), the apoenzyme C-terminal helix packs snugly against the body of the structure, making predominantly nonpolar contacts (∼75%) with the C-terminus of the α12 helix, the N-terminus of the α6 helix and the extended loop containing the α7 helix plus residues 163–175. Overall, the C-terminal helix buries 45% of its surface: approximately two-thirds against monomer *A* and one-third against monomer *B*. However, there is a network of polar interactions between several of the histidines of the His tag and both subunits of the native protein (Fig. 8*b*). The imidazole ring of His279 is parallel to and lies within 3.4 Å of the phenyl ring of Phe130. His279 is also within 2.9 Å of sulfate ion 4780, which in turn appears to interact with the N-terminal dipole of the α6 helix (within 2.8 Å). His280 is centered over and within 2.9 Å of the C-terminus of the α6 helix from the adjacent subunit, apparently interacting with the helix dipole. His283 also interacts with sulfate ion 4780. A key polar stabilizing interaction observed exclusively between native residues is the salt bridge present approximately in the middle of the interface between Lys272 and Asp159. The *B* factors in this region of the interface are also among the lowest (23–26 $Å^2$) in the entire structure. Based on the estimated helical content from CD measurements (see results presented above), this secondary-structural element may also be present in solution, although this is not certain (see earlier discussion for

details). The helix partially obstructs the binding site for NaAD in the apoenzyme (form I). In the ATP and AMP-CPP complexes, the extended His tag also partially occludes the binding site; the imidazole side chain of His279 occupies the space in the NaAD-binding site that would normally be occupied by the adenine ring of the NaAD substrate, being stabilized by π-stacking interactions with His258 (see Figs. 8*d* and 9). Remarkably, the protein is completely catalytically competent in enzymatic assays, as described earlier. A possible explanation for this apparent contradiction is that in solution the C-terminus is flexible and samples multiple conformations, one or more of which allow NaAD binding, while the conformer that crystallizes does not bind NaAD but is apparently thermodynamically favored owing to the intramolecular contacts between the C-terminus and the remainder of the protein, as shown in Fig. 8(*d*).

3.5. Packing region near the P1 loop

3.5.1. Residues 65–71. These residues include the C-terminal part of the α3 helix and a portion of the loop that immediately follows (Fig. 7*e*). The N-terminal portion of the α3 helix has a similar position in both the apoenzyme and the complexes, but the C-terminal end of the helix (Asn68) moves 1.6 Å upon complex formation. The formation of the P1 loop could play a role in the observed shift since helix α4 is contiguous with the P1 loop and also packs against the N-terminus of helix α3. There are two symmetry-related crystal contacts with residues Asn68 and Glu69 that are observed in the form II and III complexes but are not observed in this region in the apoenzyme, which may influence the change in position. A similar situation exists for the *bsu*NADS structure pair. The C^{α} position of *bsu*Glu67 differs by 1.3 Å between the *bsu*NADS apoenzyme and complex structures (PDB code 1ih8). In the case of *bsu*NADS, however, the crystallographic unit-cell and space-group parameters and therefore crystal contacts are the same for the structure pair.

3.5.2. Helix α4, residues 88–92. Residues 88–92 belong to a portion of the 11-residue helix α4 which is contiguous with the P1 loop, residues 85–87 (Fig. 7*f*). Although no direct contacts exist between residues 88–92 and the substrates, shifts in this portion of helix α4 upon complex formation may be associated with ordering of the P1 loop, which appears to translate helix α4 towards helix α3 by approximately half a turn of helix.

3.5.3. β-Strand β3, residues 101–103. Residues 101–103 comprise the N-terminal region of strand β3 and one residue preceding the strand (Fig. 7*e*). The position of strand β3 in the apoenzyme and complex structures is similar except that β3 of the complex structure is translated towards the N-terminal direction of the sheet by as much as 1.3 Å, roughly parallel to the translation observed in helix α4, which resides above it.

4. Discussion

NADS is an ubiquitous enzyme that mediates various metabolic processes. This paper describes the crystal structure of NADS from *B. anthracis* as the apoenzyme and in complexes with the ATP substrate analog AMP-CPP or the products AMP and PP_i. The primary sequence of *ban*NADS shares 77% identity with *bsu*NADS, 55% identity with *eco*NADS and 22% sequence identity with *hpy*NADS, the three other NADS enzymes for which crystal structures are available (Fig. 3). An alignment of the C^{α} atoms of all structures of the enzyme in complex with substrates indicates that *ban*NADS is very similar to *bsu*NADS (r.m.s.d. 0.42 Å) and *eco*NADS (r.m.s.d. 0.97 Å) as summarized in supplementary Table 3, with notable differences as described in the next two sections. However, there are several differences between the *H. pylori* enzyme and the other three, as exemplified by an r.m.s.d. of 1.72 Å in comparison to *ban*NADS. Fig. 10 shows a superposition of the four enzyme structures in their respective complexes.

In addition to the specific differences described in the next two sections, there are two additional, albeit small, differences between *bsu*NADS and *ban*NADS. Two regions in the *ban*NADS complex, residues 104–105 (strand β3) and 240–245 (within helix α12), deviate by more than 1 Å from the *bsu*NADS complexes (*ban*NADS numbering); this is apparently a consequence of a lack of sequence homology in these regions. Residues Val104 and Ala105 are small and hydrophobic in *ban*NADS, whereas these are substituted by the much larger hydrophobic and polar residues Trp and Lys, respectively, in the hydrophobic pocket found in *bsu*NADS. In the region 240–245 three residues are also not conserved.

4.1. Comparison of the P1 and P2 loops in different NADS structures

4.1.1. *Bsu*NADS, *eco*NADS and *ban*NADS. In all published crystal structures of *bsu*NADS and *eco*NADS apoenzymes, the P1 (85–87) and P2 (206–226; *ban*NADS numbering) loops are disordered. When the ATP-binding site is occupied by substrates or products ordering of both loops results for *bsu*NADS (Devedjiev *et al.*, 2001; Rizzi *et al.*, 1996; Symersky *et al.*, 2002), but for *eco*NADS this results in ordering of only the P1 loop (Jauch *et al.*, 2005). As in *bsu*NADS, we report here the ordering of both P1 and P2 loops in the form II and III complexes.

Jauch *et al.* (2005) suggested that crystal contacts contribute to the ordering of the P2 loop in *bsu*NADS since contacts are observed in the P2 loop in this enzyme while none are observed even near the disordered P2 loop in *eco*NADS. The role of crystal contacts is not relevant to ordering of the P1 loop, because no contacts are observed in complexes of either enzyme, both of which have ordered P1 loops. With two additional structures available since publication of the *eco*NADS structures, *hpy*NADS and *ban*NADS, it is possible to infer whether the presence of crystal contacts is required for ordering either the P1 or P2 loops in these enzymes. In the case of the P2 loop, crystal contacts are only found for one of the two molecules in the asymmetric unit of the *ban*NADS form II and III complexes; thus, the presence or absence of crystal contacts in the P2 loop region seems to be unrelated to the ordering of the P2 loop. Regarding the P1 loop, like

*bsu*NADS and *eco*NADS, there are no crystal contacts seen in the form II or III complexes of *ban*NADS.

An additional observation can be made regarding the disorder–order transition of the P1 loop by comparing the *ban*NADS and *bsu*NADS apo *versus* complex structure pairs. This is one of the two regions identified in the *ban*NADS structure as containing displacements of residues greater than 1 Å between the two pairs of structures (see Fig. 7*a*; circled residues at the bottom of the structure). Interestingly, when comparing the same region of the *bsu*NADS structures, we also see >1 Å deviations between the pairs and a similar type of shift of structural elements is responsible. We surmise that it is a consequence of the ordering of the P1 loop, which requires some conformational adjustment of nearby structural elements to accommodate the now fixed loop.

4.1.2. *Hpy*NADS *versus* *ban*NADS. In the case of *hpy*NADS, both the P1 and P2 loops are ordered in both the apo and complex structures (Kang *et al.*, 2005); however, the sequence homology is much lower than for the other three homologs (see Fig. 3). The P2 loop is also shorter, lacking three residues at the tip of the loop, and while crystal contacts are found in the P2-loop region of the apoenzyme structure, only one of the two molecules in the asymmetric unit of the complex shows a weak (3.14 Å) crystal contact. On the other hand, the P1 loop is longer in *hpy*NADS, contains no identical residues and only slim homology to the other three homologs, but nevertheless the 'P1' loop residues do occupy the same region of space in the structure. While it is ordered in both the apoenzyme and complex structures, it exhibits no crystal contacts in either form. Thus, crystal contacts do not play a role in ordering the 'P1' and P2 loops of *hpy*NADS.

In conclusion, by comparing all structures, there seems to be no consistent trend implicating a role for crystal contacts in ordering either the P1 or P2 loops in these enzymes.

4.1.3. ATP-binding site comparison: *bsu*NADS. The ATP-binding site of *ban*NADS is strikingly similar to that of *bsu*NADS. Fig. 6(*a*) shows a superposition of all the residues involved in binding AMP-CPP, Mg^{2+}-II and Mg^{2+}-III in the two enzymes (from the *bsu*NADS structure; PDB code 1ih8). Not only are all the active-site residues conserved, but there is very limited difference in the conformations adopted by these residues.

A notable difference between the complexes of *bsu*NADS and *ban*NADS is the difference in Mg^{2+} occupancy (summarized in supplementary Table 2). The location of Mg^{2+}-III in *bsu*NADS is shifted 3.0 Å towards the NaAD-binding site relative to the Mg^{2+}-I site. This Mg^{2+}-III site was suggested to be the catalytic site or an intermediate site, since these crystals were grown not at the usual pH 5.2 but at pH 7.5, which is closer to the optimal pH for the enzymatic reaction (pH 8.5; Devedjiev *et al.*, 2001). However, the crystal structure of *ban*NADS (crystals grown at pH 7.0) does not show the presence of the Mg^{2+}-III ion.

4.1.4. ATP-binding site comparison: *eco*NADS. The ATP-binding sites of *ban*NADS and *eco*NADS are quite similar and all of the binding-site residues are conserved, as previously reported for the comparison of *eco*NADS with *bsu*NADS (Jauch *et al.*, 2005). The only notable difference, as previously described (Jauch *et al.*, 2005), is that the P2 loop remains disordered in the *eco*NADS structure and therefore no interactions between Thr211 (*eco*NADS numbering) and the Mg^{2+}-II or PP_i ions are observed. Both the *ban*NADS and *eco*NADS complex structures with AMP and PP_i have Mg^{2+} ions in both the Mg^{2+}-I and Mg^{2+}-II sites.

4.1.5. ATP-binding site comparison: *hpy*NADS. To date, there are no reported *hpy*NADS complex structures with AMP or PP_i and the only reported complex structure with ATP and NaAD has only one Mg^{2+} ion per monomer, which occupies the Mg^{2+}-II site (PDB code 1xng; Kang *et al.*, 2005). The ATP-binding site of the *hpy*NADS complex structure is similar to that of *ban*NADS, but there are a few differences worth mentioning here (as described in Kang *et al.*, 2005). The majority of the binding-site residues are conserved between the two species, with the following differences (see supplementary Table 2): Gln50 in *ban*NADS *versus* Leu36 in *hpy*NADS, Arg79 in *ban*NADS *versus* Leu57 in *hpy*NADS and Gln85 in *ban*NADS *versus* Met64 in *hpy*NADS. Since the main-chain atoms are responsible for the interaction between Gln50 in *ban*NADS and PP_i, this interaction is conserved, *i.e.* the main-chain N atom of Leu36 in *hpy*NADS interacts with the phosphate moiety of ATP. All but two interactions with ATP found in the other three homologous structures are maintained in *hpy*NADS *via* an interaction with the same or a homologous side-chain residue.

4.2. Comparison of the C-terminus of apo *ban*NADS to other NADS structures

As presented in §3, the non-native C-terminal extension, containing the sequence ^{273}LAAALEHHHHHH^{284}, recruits native residues to form an extended helix from residues 267–282, whereas the C-termini of the *ban*NADS form II and III complex structures are mostly random coil and are reminiscent of the C-termini observed in the *B. subtilis* and *E. coli* NADS structures (Fig. 10).

The stabilizing interactions observed between the C-terminal helix of the *ban*NADS apoenzyme and the rest of the protein, as described in §3, are apparently significant enough to cause conformational adjustments in this region of the structure (Figs. 7 and 8). The formation of the C-terminal helix, with its concomitant interactions, overrides the native-like secondary structure for this region that is exhibited in the complexes of *ban*NADS, as well as *bsu*NADS, either as the apoenzyme or in complexes. Progressing along the sequence from residues in the C-terminal helix to those in the first native-like helix, α11, *B* factors systematically and continually increase until the stretch of residues 265–257, which are completely disordered in the apoenzyme structure; immediately after this gap, residues in helix α12 appear starting at 266. At this point, the displacement of the α12 helix in the apoenzyme from the native-like position seen in the complexes of *ban*NADS is rather large, $\sim$4 Å. Smaller displacements from the norm are observed in the regions remote from the C-terminal helix.

It seems likely that the relaxation from the non-native positions in the apoenzyme to more native positions is forced by the energetically favorable binding of the ATP substrate (catalytically hydrolyzed to AMP and PP_i; crystal form II) or substrate analog AMP-CPP (form III). A comparison of the apoenzyme (form I) and complex crystal structures suggest a mechanism for the relaxation that probably starts with a steric clash between the substrate phosphate O atom and the side chain of Lys171, which are within 2 Å in the two forms. Upon ordering of the P2 loop over the substrate, a constellation of steric clashes would also exist with the apoenzyme conformation of key aromatic residues that are present in the inner loop (residues 158–176), namely Phe168, Phe169 and Phe172. In the complex forms, the P2 loop packs against this inner loop and forces it to move into a more favorable conformation in which the side chains of all these three residues rotate and translate to avoid steric overlaps. This displacement in turn allows further adjustments of helices α1, α11 and α12 to relax into the core of the structure. Therefore, the displacement of the inner loop plays a crucial role by creating the necessary space to adopt a native-like structure.

As shown in Fig. 7(*d*), the C-terminus of helix α12 of the form II and III complexes and residues 255–260 share common space with the C-terminal helix of form I. This requires an adjustment of the C-terminal helix position in the complexes. Since the C-terminal helix is largely buried in the apoenzyme structure, there is no obvious way for it to move out of the way and it probably unfolds before adopting the catalytically active structure observed in the form II and III complexes. As noted in §3, the residues 257–265 that are disordered in the apoenzyme *ban*NADS structure are not disordered in the crystal structures of the other known apoenzyme NADS, nor are they disordered in the *ban*NADS complexes (Fig. 7*d*). A consequence of their implied flexibility would be the ability of residues 257–265 to act as a hinge during the transition from apoenzyme to complex.

4.3. Significance of the structured His tag of *ban*NADS

Two of the published NADS structures were derived from constructs containing a histidine tag, namely *hpy*NADS, which has a non-interacting C-terminal His tag extending away from the NaAD-binding site (Kang *et al.*, 2005), and *eco*NADS, which has an N-terminal His tag that is disordered and not observed in the crystal structures reported (Fig. 10). The observation of a His tag in the crystal structure of any protein is rare; of 13 048 structures in the PDB deposited between 1995 and 2005, only 1142 of the derived proteins contain His tags and of these only 65 (less than 6%) of the structures actually contain observable coordinates for at least the main chain of four or more consecutive histidines (Carson *et al.*, 2007).

To our knowledge, the apoenzyme *ban*NADS structure is one of only two known structures that show non-native conformations that result directly from the presence of the His tag. The other published structure is the DraD invasin from uropathogenic *E. coli* (PDB code 2axw; Carson *et al.,* 2007). The presence of 13 additional residues, including the His tag, at the C-terminus, apparently induces the formation of a dimer with swapped β-strand C-termini. Unlike the DraD invasin protein and *ban*NADS, other structurally observed His tags show interactions with either a subunit partner or a symmetry-related molecule (Carson *et al.*, 2007).

The authors would like to thank Debbie McCombs for preliminary crystal screening, Zhengrong Yang for crystallization scale-up and Carol Parr for growing crystals. We would also like to thank the Southeast Regional Collaborative Access Team staff at the Advanced Photon Source in Chicago, IL, USA. DNA sequencing was carried out by the CFAR DNA Sequencing Core at UAB with the NIH CFAR Core grant P30A127767. This work was supported by NIH Grant U01 AI 56477.

References

Bergmeyer, U. (1974). Editor. *Methods of Enzymatic Analysis*, Vol. 4, pp. 2048–2050. New York: Academic Press.
Böhm, G., Muhr, R. & Jaenicke, R. (1992). *Protein Eng.* **5**, 191–195.
Brünger, A. T., Adams, P. D., Clore, G. M., DeLano, W. L., Gros, P., Grosse-Kunstleve, R. W., Jiang, J.-S., Kuszewski, J., Nilges, M., Pannu, N. S., Read, R. J., Rice, L. M., Simonson, T. & Warren, G. (1998). *Acta Cryst.* D**54**, 905–921.
Carson, M. (1997). *Methods Enzymol.* **277**, 493–505.
Carson, M., Johnson, D., McDonald, H., Brouillette, C. & DeLucas, L. (2007). *Acta Cryst.* D**63**, 295–301.
Copley, R. & Barton, G. (1994) *J. Mol. Biol.* **242**, 321–329.
DeLano, W. (2002). *The PyMOL Molecular Graphics System.* DeLano Scientific, Palo Alto, CA, USA. http://www.pymol.org.
Devedjiev, Y., Symersky, J., Singh, R., Jedrzejas, M., Brouillette, C., Brouillette, W., Muccio, D., Chattopadhyay, D. & DeLucas, L. (2001). *Acta Cryst.* D**57**, 806–812.
Hutchinson, E. G. & Thornton, J. M. (1996). *Protein Sci.* **5**, 212–220.
Jauch, R., Humm, A., Huber, R. & Wahl, M. (2005). *J. Biol. Chem.* **280**, 15131–15140.
Jones, S. & Thornton, J. (1996). *Proc. Natl Acad. Sci. USA*, **93**, 13–20.
Jones, T. A., Zou, J.-Y., Cowan, S. W. & Kjeldgaard, M. (1991). *Acta Cryst.* A**47**, 110–199.
Kang, G., Kim, S., Im, Y., Rho, S., Lee, J. & Eom, S. (2005). *Proteins*, **58**, 985–988.
Lovell, S., Davis, I., Arendall, W. III, de Bakker, P., Word, M., Prisant, M., Richardson, J. & Richardson, D. (2003). *Proteins*, **50**, 437–450.
McCoy, A. J., Grosse-Kunstleve, R. W., Storoni, L. C. & Read, R. J. (2005). *Acta Cryst.* D**61**, 458–464.
McDevitt, D., Payne, D., Holmes, D. & Rosenberg, M. (2002). *J. Appl. Microbiol.* **92**, 28S–34S.
Magni, G., Amici, A., Emanuelli, M., Raffaelli, N. & Ruggieri, S. (1999). *Adv. Enzymol. Relat. Areas Mol. Biol.* **73**, 135–182.
Morris, R. J., Perrakis, A. & Lamzin, V. S. (2003). *Methods Enzymol.* **374**, 229–244.
Nessi, C., Albertini, A., Speranza, M. & Galizzi, A. (1995). *J. Biol. Chem.* **270**, 6181–6185.
Otwinowski, Z. & Minor, W. (1997). *Methods Enzymol.* **276**, 307–326.
Potterton, E., Briggs, P., Turkenburg, M. & Dodson, E. (2003). *Acta Cryst.* D**59**, 1131–1137.

Read, T. *et al.* (2003). *Nature (London)*, **423**, 81–86.
Rizzi, M., Bolognesi, M. & Coda, A. (1998). *Structure*, **6**, 1129–1140.
Rizzi, M., Nessi, C., Mattevi, A., Coda, A., Bolognesi, M. & Galizzi, A. (1996). *EMBO J.* **15**, 5125–5134.
Rizzi, M. & Schindelin, H. (2002). *Curr. Opin. Struct. Biol.* **12**, 709–720.
Sali, A. & Blundell, T. L. (1993). *J. Mol. Biol.* **234**, 779–815.
Schwede, T., Kopp, J., Guex, N. & Peitsch, M. C. (2003). *Nucleic Acids Res.* **31**, 3381–3385.
Shailubhai, K. (2003). *IDrugs*, **6**, 773–780.
Spencer, R. & Preiss, J. (1967). *J. Biol. Chem.* **242**, 385–392.
Symersky, J., Devedjiev, Y., Moore, K., Brouillette, C. & DeLucas, L. (2002). *Acta Cryst.* D**58**, 1138–1146.
Velu, S., Cristofoli, W., Garcia, G., Brouillette, C., Pierson, M., Luan, C., DeLucas, L. & Brouillette, W. (2003). *J. Med. Chem.* **46**, 3371–3381.
Velu, S., Luan, C., DeLucas, L., Brouillette, C. & Brouillette, W. (2005). *J. Comb. Chem.* **7**, 898–904.
Zalkin, H. (1985). *Methods Enzymol.* **113**, 297–302.